Macromolecules

pubs.acs.org/Macromolecules Article

Characterizing Nonuniform Hydrogel Elastic Moduli Using Autofluorescence

John A. McGlynn and Kelly M. Schultz*

Cite This: *Macromolecules* 2022, 55, 4469−4480 Read Online

ACCESS | Metrics & More | Article Recommendations | Supporting Information

ABSTRACT: Hydrogel biomaterials show promise as implantable cell delivery vehicles that enhance tissue regeneration and the natural healing process. The design of these materials requires that they mimic the natural environment to retain native cell function. Biological tissues often have spatially varying stiffness, allowing them to have a variety of functions within the body. However, this makes them challenging to mimic mechanically with a synthetic scaffold. To enable these complex designs, characterization techniques that measure nonuniform mechanical properties are required, but these methods are limited. Bulk rheological measurements average the stiffness of the sample, microrheological methods cannot characterize high moduli materials (despite being able to resolve spatial variability), and atomic force microscopy measurements can be a function of the selected tip geometry and measurement procedure. We present a new method for determining the stiffness of nonuniform hydrogels. Our technique measures the hydrogel's autofluorescent brightness, which is related to its degree of cross-linking, and relates this brightness to elastic modulus. We use a well-established 3D cell encapsulation platform. This photopolymerized polymer−peptide hydrogel is composed of poly(ethylene glycol)−norbornene and a matrix metalloproteinase (MMP)-degradable peptide. We first develop a relationship between hydrogel elastic modulus and brightness, which are systematically varied by controlling UV light exposure during photopolymerization. We then relate elastic modulus and autofluorescent brightness at each exposure time. This relationship enables images of hydrogels that measure brightness to be converted into stiffnesses. To demonstrate the technique, we fabricate hydrogels with nonuniform stiffness profiles: (1) step changes and (2) smooth gradients in elastic moduli. These are made by controlling UV light exposure spatially with a photomask. We then characterize these gels with the new technique. This work provides an alternative characterization method for hydrogels with spatially nonuniform stiffnesses. To effectively design materials for cell encapsulation, they must be characterized so that their properties are finely tuned to match native tissue. This will improve the effectiveness of these scaffolds as cell delivery vehicles and in promoting tissue regeneration.

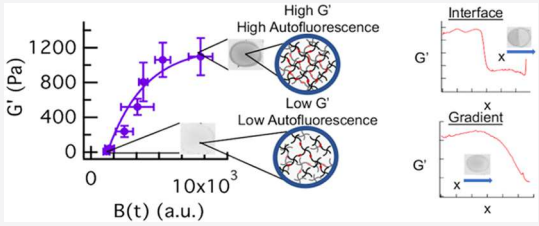

INTRODUCTION

Hydrogels are being designed with increasing complexity to mimic the environment of native tissue so that they can serve as a temporary niche for the delivery of cells or drug molecules to the body.[1−13] A goal of these materials is to implant them at the wound site laden with cells; these cells would migrate out of the material and into the wound to conduct healing, and the scaffold provides structure to the wound.[14,15] A particularly attractive cell type for targeted cell delivery at a wound site are human mesenchymal stem cells (hMSCs), which improve the rate and outcome of healing. These cells coordinate the healing process by calling the appropriate cells to the wound and can also differentiate into the cell type of the wounded native tissue.[16,17] Previous work has shown that hMSCs specify a lineage based, in part, on the physical stiffness of their surroundings.[1,4,18,19] Because of this, it is important that an implant provide a similar stiffness as the native tissue so that hMSCs commit to the correct lineage. To mimic native tissue, which is generally spatially heterogeneous in stiffness, fabrication methods that enable precise spatial control over implant stiffness are required. Additionally, a characterization method for these spatially nonuniform materials will be necessary to verify that desired rheological properties are achieved. In this work, we provide a technique for fabricating and characterizing materials with complex spatial stiffness profiles.

Many of the unique and highly variable properties of biological materials can be attributed to their mechanical properties.[20,21] In this work, we have chosen to focus on the development and characterization of interfaces between different rheological properties and smooth stiffness gradients. In the body, tissues of different mechanical properties create an interface where spatial mechanical properties change rapidly, such as where bone meets cartilage.[22,23] Matching these rapid

Received: January 31, 2022
Revised: April 28, 2022
Published: May 16, 2022

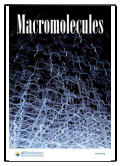

https://doi.org/10.1021/acs.macromol.2c00241
Macromolecules 2022, 55, 4469−4480

changes in mechanical properties is especially important when using hydrogels as implantable cell delivery tools for wound repair. As the cells remodel and degrade their microenvironment, they will eventually leave the material and enter the native tissue. This requires that they traverse an interface where mechanical properties change rapidly.[22,24,25] Mechanical properties of biological materials can also change in a smooth gradient.[22,25] Connective tissue, such as tendons, ligaments, and fascia, can have elastic moduli, G', which varies with a steep gradient.[22] For example, in the anterior cruciate ligament (ACL) stiffness increases rapidly in a gradient as the bone is approached due to a rapid increase in mineralization.[22] While the ACL is a frequently injured area of the body and would benefit from repair using implantable hydrogels, mimicking the ACL's natural gradient presents a challenge. To repair these tissues, the stiffness of the hydrogel must mimic that of the native tissue so delivered cells respond and commit to the correct lineage, and the hydrogel provides mechanical support similar to the damaged tissue.

hMSCs are integral to the healing process, controlling and orchestrating wound progression and differentiating into the cell type of the native tissue.[16,17,26] Mechanical stiffness has a significant impact on the behavior and function of hMSCs. Stem cell migration rates and remodeling are significantly impacted by the moduli of their surrounding material.[27,28] Previous work has shown that the structure, remodeling, and behavior of migrating hMSCs change based on pericellular stiffness.[1,27,28] As hydrogel stiffness increases, hMSC secretions also change to enable basic processes, including migration. hMSCs secrete more proteolytic enzymes when encapsulated in stiffer materials.[29] This is important because many implantable hydrogels are designed to be degraded by these enzymes, and this change in secretions will change hMSC-mediated scaffold degradation.[27,29] Finally, cell morphology is also governed in part by substrate material properties, and this morphology is important in effective cell migration and function. Cells must be able to extend into their surrounding material and attach to pull themselves forward during migration. This requires that they change their shape into a more extended morphology. Tse and Engler fabricated hydrogels with stiffness gradients and measured that cells seeded on stiffer substrates had more extended morphology while those on softer substrates remained more rounded.[18] This indicates that cells in different areas of the gradient will migrate at different rates, impacting delivery out of the material and into the native tissue. Because of the importance of the initial stiffness of the material on hMSC function, accurately fabricating and characterizing materials is important in designs that use their stiffness to direct hMSC basic processes.

Many traditional methods for characterizing mechanical stiffness are not able to characterize spatially nonuniform materials. Bulk rheological methods using small amplitude oscillatory shear, a standard method for characterizing material stiffness, result in an average measurement of the material contacted by the geometry.[30] This prevents it from being used to characterize materials where stiffness is changing spatially. Microrheological measurements can measure the modulus of materials in small fields of view which could be taken at different positions in the sample to measure spatial variation; however, these measurements are limited to very soft materials with $G' \lesssim 4$ Pa. This prevents microrheological measurements from being used to characterize material stiffnesses that mimic most tissues in the body.[31−33] Atomic force microscopy (AFM) is another technique that has been used to quantify material stiffness. AFM measurements are influenced by tip geometry and material heterogeneity. Additionally, they risk damaging the material during the measurement, which is especially relevant for softer materials, and are limited in their scan area.[34−37] To overcome these limitations, we present a new measurement technique that quantifies hydrogel elasticity using autofluorescence. This technique uses images of hydrogel autofluorescence collected by a high-resolution scanner and relates spatial variations in brightness in the image to variations in elastic modulus, G'. An advantage of this technique is that it does not require the addition of a fluorophore since innate autofluorescence of the material is characterized.

Autofluorescence is the intrinsic fluorescence emitted by a molecule that is not intended to be a fluorescent marker.[38] Autofluorescence is often an undesirable property of materials because it complicates the use of fluorescent molecules. When the brightness of fluorescent molecules is similar to the background autofluorescence of a sample, it prevents meaningful measurements. An example of this is when the autofluorescence of a sample chamber competes with the fluorescent signal of dye molecules in a sample. If the concentration of dye in the sample is low, it will become comparable with the fluorescence of the container and will be indistinguishable from the background. Recently, autofluorescence of a variety of different hydrogels has been measured to directly correlate with extent of gelation and indirectly correlate with water content.[39] Results by Xu et al. show that these phenomena are similar to aggregation-induced emission (AIE), a property originally observed for some small molecules.[39−43] Some molecules that are not fluorescent when free in solution, such as in a good solvent, become fluorescent as they aggregate when solvent quality decreases.[40,43] This fluorescence arises because the molecules are no longer able to dissipate energy gained from incoming photons through molecular motion and must instead re-emit at a longer wavelength, resulting in fluorescence.[40,43] This same phenomenon occurs in a gel when the motion of polymer chains becomes restricted during gelation.[39] As a gel forms, more polymer becomes cross-linked in an increasingly dense network, and the space available for polymer motion is reduced. Additionally, the ability for the polymers to move is hindered because of the attachment to the network. The cross-linking of polymer chains results in an increase in modulus and an increase in fluorescence due to reduced molecular motion of the chains. Because both moduli and autofluorescence are related to cross-link density, an increase in fluorescence can be related to an increase in modulus. In this work, we correlate the change in fluorescence to the increase in elastic modulus of our material. This allows us to image a gel and convert a brightness measurement into an elastic modulus. Additionally, the brightness of the image is measured on the order of pixels, enabling high-resolution spatial measurements of mechanical stiffness.

In this study, we develop a new technique to characterize materials with spatially varying rheological properties. Our target moduli is controlled by the range of stiffnesses possible for our chosen hydrogel scaffold. Depending on the cross-linker to backbone ratio and UV exposure time, this hydrogel can have moduli of $G' \approx 0-2.5$ kPa.[27] This range of stiffnesses mimics a variety of tissues, from neural to endothelial tissue.[21] We develop the technique using a model photopolymerized hydrogel used widely for cell encapsulation.[8,28,44−52] This

https://doi.org/10.1021/acs.macromol.2c00241
Macromolecules 2022, 55, 4469−4480

polymer−peptide hydrogel is photopolymerized at varying cross-link densities by varying UV exposure time. We then measure the elastic modulus and autofluorescent brightness as a function of UV exposure time in spatially uniform hydrogels. We use these measurements to develop a relationship between hydrogel elastic modulus and autofluorescent brightness. We then form hydrogels with step changes and gradients in G' by spatially controlling UV exposure time with a photomask. These nonuniformities in stiffness are then analyzed by measuring hydrogel autofluorescence spatially and using our developed relationship to calculate G'. This technique enables fabrication and characterization of materials with spatially nonuniform properties, which will enable implantable scaffolds to be designed to better mimic the native microenvironment and improve their function for wound healing and tissue regeneration applications.

MATERIALS AND METHODS

Hydrogel Formulation. All hydrogel components are dissolved in phosphate buffered saline (PBS, 1× , Gibco), unless otherwise stated. The given concentration is the concentration in the final precursor solution. After solutions of each component are made, they are mixed together prior to gelation. The final composition of our precursor solution contains poly(ethylene glycol)−norbornene (PEG-N), a peptide cross-linker, and a photoinitiator. The hydrogel backbone is a 4-arm star PEG-N (f = 4, where f is the number of functional groups, 3 mM, M_n = 20,000 g mol^{-1}, JenKem). These backbone molecules are cross-linked with a peptide, *KCGPQG↓IWGQCK* (f = 2, 3.9 mM, Bachem), by a radically mediated thiol−ene photopolymerization.[51−54] This peptide cross-linker is cleaved by cell-secreted enzymes called matrix metalloproteinases (MMPs).[15,55] This makes the material well-suited for studying cell−material interactions because it allows cells to remodel the material during basic processes, such as migration. Radicals are produced when the photoinitiator lithium phenyl-2,4,6-trimethylbenzoylphosphinate (LAP, 1.7 mM) in the solution is exposed to UV light at 365 nm initiating the cross-linking reaction. LAP is synthesized using previously published protocols.[52] The precursor solution is injected into a sample chamber, which is described in the next section, prior to UV light exposure.

Sample Chamber Fabrication. Two types of sample chambers are used for this study: one for preparing 100 μL hydrogels for bulk rheology and one for preparing 34 μL hydrogels for fluorescence measurements. Each sample chamber consists of a polydimethylsiloxane (PDMS, Dow Corning) ring which holds the precursor solution prior to gelation so that a consistent gel shape is made. The ring is cut from a sheet of PDMS made in a Petri dish (150 × 50 mm, Corning). The sheet is made by mixing a silicone elastomer base with a cross-linker in a 1:10 ratio, which is recommended by the manufacturer. The ring is cut from the sheet using biopsy punches (Integra Biosciences), which set the outer and inner diameter of the ring. The outer diameter is 10 mm for all sample chambers. The inner diameter is 6 mm in sample chambers used for fluorescence measurements and 8 mm for sample chambers used for bulk rheology measurements. The ring is attached to a glass slide (25 × 75 × 1 mm, Fisher Scientific Company) by UV-curable adhesive (Norland Optical Adhesive NOA81, Norland Optical Products). After the gel is photopolymerized, the ring can be easily removed, allowing the gel to swell uniformly on the glass slide when it is immersed in PBS.

Uniform Gel Formation. UV light for gel formation is provided by a light-emitting diode (LED) UV lamp (M365LP1-C1, Thor Laboratories Inc.). Prior to setting the light intensity, a 3D-printed collimator tube is placed on the lamp to collimate the light to a beam 10 mm in diameter, matching the size of the PDMS ring. This ensures that light is exposed uniformly across the sample and is focused only on the sample. A schematic of the setup is shown in Figure 1. After attaching the collimator, the light intensity is set to 1.5 mW cm^{-2} using a LED driver (LEDD1B, Thor Laboratories Inc.) and a UV radiometer (Sper Scientific).

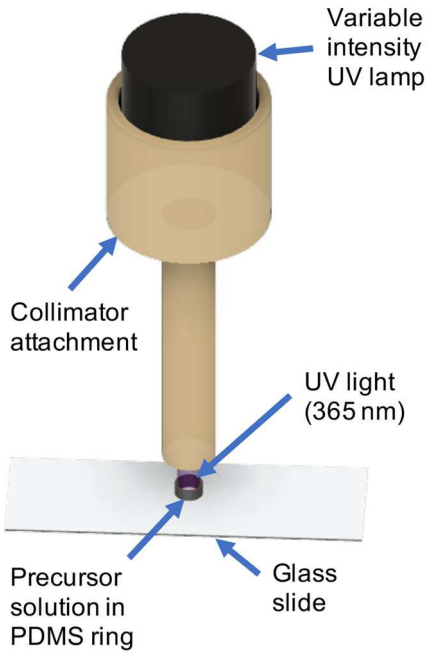

Figure 1. Schematic of the lamp and collimator over a sample being exposed to UV light. This schematic is not to scale.

After the UV light is calibrated, the precursor solution is injected into the center of the PDMS ring in the sample chamber. The sample chamber is then placed under the UV light in the same location previously used to calibrate the UV intensity. The precursor solution is exposed for a specified amount of time (25−300 s) and then removed. The PDMS ring is removed using a spatula and tweezers, and then the glass slide with the sample on it is placed in a recrystallizing dish (Pyrex) filled with PBS to swell. Gels are left to fully swell on a laboratory bench for at least 4 h before measurements are taken.[47] We do not expect G' or autofluorescent intensity to change significantly over time after swelling because the structure of the hydrogel only changes very slowly (on the time scale of days to weeks) due to hydrolysis.[47]

Bulk Rheology. The hydrogel elastic modulus (G') is measured using a bulk rheometer (Ares G2, TA Instruments). An 8 mm sandblasted parallel plate is used as the geometry. The plate is sandblasted to minimize slip during the measurement. Because the hydrogels expand during swelling, an 8 mm biopsy punch is used to cut the swollen gel so that the sample is the same size as the geometry. A frequency sweep is then performed at 1% strain from 0.1 to 20 Hz at 37 °C. This temperature is chosen to accurately measure gel moduli at the same conditions as cell-laden scaffolds. These measurement parameters are selected based on previous work with the same hydrogels.[47] Measurements of individual gels are taken by averaging G' at all frequencies in the linear viscoelastic regime identified as the range of frequencies where G' does not change with frequency. This is typically from 0.1 to 1 Hz for these hydrogels. The upper bound of this frequency range decreases at shorter UV exposure times since the gels are weaker. Data are reported as the average of nine gel measurements plus or minus the standard deviation. All frequency sweep data are available in the Supporting Information (Figure S1).

Fluorescence Measurements. We quantify the intrinsic fluorescence, or autofluorescence, of our hydrogel at different extents of reaction, which is varied by changing UV exposure times. These brightness measurements are then related to G'. Prior to measuring autofluorescence, slides with hydrogels on them are removed from a recrystallizing dish where they are incubated in PBS. Hydrogel autofluorescence is measured using a GE Amersham Typhoon laser

https://doi.org/10.1021/acs.macromol.2c00241
Macromolecules 2022, 55, 4469−4480

scanner (Cytiva). Laser voltage is set to 600 V, and a Cy2 laser/filter combination is used. Sample chamber slides are placed in the laser scanner and imaged at a resolution of 25 μm per pixel. The resultant image is exported as a TIFF file and analyzed. The autofluorescence of a glass slide is measured in separate experiments and is insignificant compared to the autofluorescence of a hydrogel. A complete set of images used to measure brightness for uniform hydrogels are provided in Figure S2. All images for interface and gradient hydrogels are provided in Figures S3 and S4.

Interface Formation. Hydrogels with step changes in G' (we will refer to these as materials with interfaces) are formed using a photomask (PhotomaskPORTAL), which prevents UV light exposure to half of the gel. The photomask is a transparency printed at 40,000 dots per inch. The half of the gel not covered by the photomask is exposed for the entire UV exposure time. The photomask is quickly removed during UV exposure to expose the other half of the precursor solution for a desired amount of time. After UV exposure, gels with interfaces are swollen in PBS for at least 4 h and imaged to measure autofluorescence. Three different interfaces are formed in this work: (1) 300 s/120 s, (2) 300 s/30 s, and (3) 120 s/30 s where the first time is the UV exposure time on the half of the hydrogel that is exposed for the entire polymerization and the second time is the UV exposure time for the half of the hydrogel that is initially under the photomask.

Gradient Formation. Gradients are formed by moving a photomask over the precursor solution at a constant speed using a syringe pump (New Era Pump Systems). This creates a linear change in UV exposure across the sample which results in a gradient in G'. The setup for creating a gradient is shown in Figure 2. The speed the photomask is moved across the precursor solution is controlled by changing the pumping rate of the syringe pump.

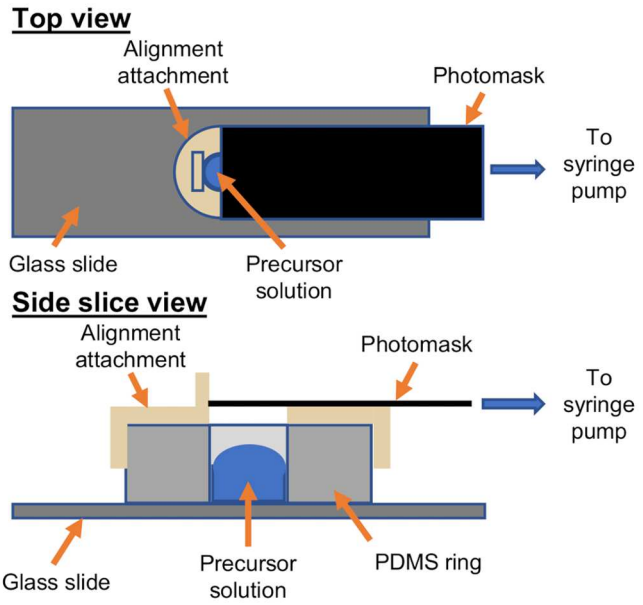

Figure 2. Schematic of the setup for creating a gradient in G'. The photomask is attached to a syringe pump which pulls it at a constant rate. The photomask is aligned using an alignment attachment to ensure that it consistently starts at the leftmost edge of the precursor solution.

Initially the receding edge of the photomask is aligned at the inner edge of the PDMS ring to cover the entire precursor solution. This alignment is achieved using a custom-made 3D-printed alignment attachment that attaches to the PDMS ring and provides a straight edge for the photomask to rest against (Figure 2). The precursor solution is exposed the moment the syringe pump begins pulling the photomask.

Three different gradients are formed in this work: (1) 180−30 s, (2) 120−30 s, and (3) 60−45 s. The first time refers to the maximum UV exposure time which occurs at one edge of the hydrogel while the second time refers to the minimum UV exposure time which occurs at the opposite end of the gel. Ideally, there is a linear change in UV exposure time across the sample between these two values. After gelation, the PDMS ring is removed, and the slide is immersed in PBS for at least 4 h to fully swell the hydrogel.

Image Analysis. Analysis of hydrogel images is done in MATLAB R2020a (MathWorks) using TIFF files produced by the laser scanner. The image that is saved is an image of sample chambers with gel samples on each slide. After the image is loaded into MATLAB, the region of interest (a single gel on a slide) in the image is zoomed in on so that the pixels which are part of the gel can be accurately selected. The outer edges of the gel are traced, defining a polygon region of interest whose interior points are analyzed for their brightness.

The image produced by the laser scanner prior to export has pixels with 100,000 possible values. When this image is exported into the TIFF file format, a square-root transform converts the pixel values from the range 0−100,000 to the pixel value range of the TIFF file format, which is 0−65,535. Prior to analysis of the pixel values in the gel image, we revert the image to the original pixel values (0−100,000). We use the untransformed data in this work because it is not distorted by the transform and provides more granularity in the brightness measurement. Once the transform is undone and the region of interest for a gel is defined, the brightness values of all pixels within the selected region are converted to G' using a relationship that will be discussed in the Results and Discussion section.

Experimental Design. Data collection for the calibration curve that relates autofluorescence to elastic moduli is as follows. A single, large precursor solution is used to create 12 gels for autofluorescence and 12 gels for bulk rheometry. After the experiment is complete, N = 3 measurements are collected for the selected UV exposure times. Experiments are repeated until three sets of three gels are measured at each exposure time for both autofluorescence and G'. This results in a total of N = 9 measurements for each variable. Each set of three gels for a given UV exposure time is formed from a different stock solution to measure solution to solution variability.

Data collection for interfaces and gradients is as follows. A single precursor solution is used to create three gels: one of each of the UV exposures which gives an interface or one of each of the UV exposures which gives a gradient. These gels are measured for their brightness and analyzed. Experiments are repeated until N = 3 gels of each interface and N = 3 gels of each gradient are measured. Each gel (gels 1−3) is made from a different stock solution.

Data Analysis and Statistics. Curve fitting for Figure 3 is done in Igor Pro (Wavemetrics). The data in Figures 3a,b are fit using least-squares fitting with weighting where the weights applied at each point are the standard deviations. Because Figure 3c has standard deviations in both their x and y variables, the fit considers both in the weighting. This is done using orthogonal distance regression, which minimizes the orthogonal distance between each point and the fitted curve while also taking into account weightings for the standard deviations in both variables.[56]

RESULTS AND DISCUSSION

The goal of this work is to develop a method that relates hydrogel autofluorescence, $B(t)$, to elastic modulus, $G'(t)$, and demonstrate this technique by characterizing spatially nonuniform hydrogels. We use hydrogel autofluorescence because it is easily measured, and the hydrogel is chemically and mechanically unaffected by the measurement. Our results for this hydrogel platform measure that the change in $G'(t)$ as a function of UV exposure time follows first-order reaction kinetics, and the brightness from hydrogel autofluorescence is linearly correlated to UV exposure time. We combine these two relationships to relate G' to autofluorescence. We then successfully characterize the spatial moduli of nonuniform gels

https://doi.org/10.1021/acs.macromol.2c00241
Macromolecules 2022, 55, 4469−4480

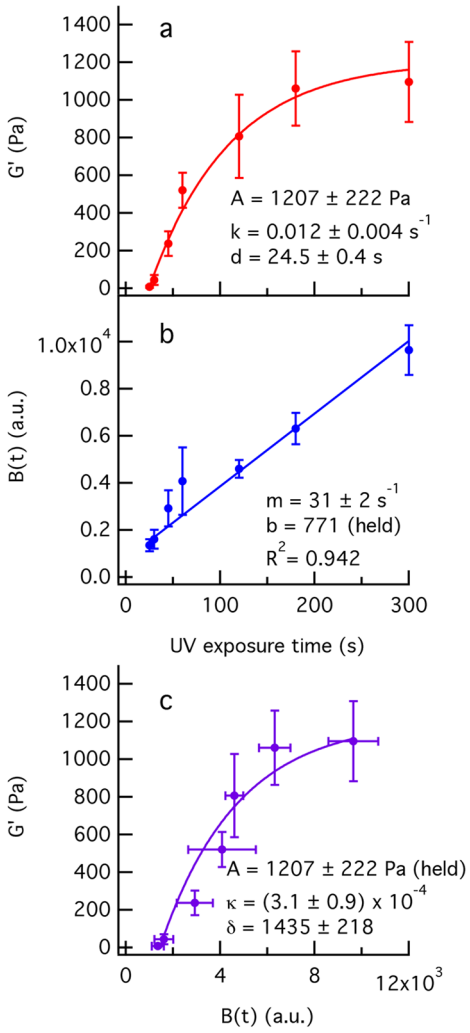

Figure 3. Calibration curves for how (a) elastic modulus, $G'(t)$, and (b) gel autofluorescence, $B(t)$, changes with UV exposure time, t. (c) The resulting relationship between $G'(t)$ and $B(t)$.

using autofluorescence measurements and the previously established relationship. These results demonstrate that measurements of autofluorescence can be used to accurately determine spatial variation in G' in a variety of hydrogels with nonuniform stiffness.

Development of the Measurement Technique. We develop a relationship between $G'(t)$ and $B(t)$ by measuring each at different extents of gelation or UV light exposure time, t. The results are provided in Figure 3. We react precursor solutions for a given t and then measure the elastic modulus of each partially reacted uniformly exposed gel on a bulk rheometer using a frequency sweep and measure the autofluorescence with a laser scanner. The results of bulk rheology and brightness measurements are shown in Figures 3a and 3b, respectively. The change in $G'(t)$ with UV exposure time, t (Figure 3a), follows first-order reaction kinetics and is fit to

$$G'(t) = A\left[1 - e^{-k(t-d)}\right] \quad (1)$$

The three fit parameters are A, k, and d. A is the modulus (Pa) of the fully reacted gel at equilibrium, k is the reaction rate constant (s^{-1}), and d is a delay time (s). d is the time required after initially exposing the sample to UV light for $G'(t)$ to become measurable. This requires radicals to build up in the system initiating the gelation reaction and the reaction to proceed until the material has a measurable elastic component. Our shortest UV exposure time, 25 s, is very close to the value of d, indicating that we are forming gels very close to a measurable G' with bulk rheology. These fit parameters provide an accurate relationship between $G'(t)$ and UV exposure time, enabling prediction of one from the other. We next measure how hydrogel autofluorescence, $B(t)$, varies with UV exposure time.

Hydrogel autofluorescent brightness, $B(t)$, varies linearly with UV exposure time (Figure 3b). We fit $B(t)$ vs t using the equation

$$B(t) = mt + b_0 \quad (2)$$

where m is the slope of the line with units of s^{-1} and b_0 is the intercept. The intercept, b_0, is the brightness of a gel with zero UV exposure. We set b_0 to be the average background brightness of a glass slide and only fit the value of m. m describes the rate at which polymer chains lose mobility due to cross-linking into the forming gel network. These chains then contribute to the measured autofluorescence by aggregation-induced emission.

Measurements of uniform stiffness gels at varying UV exposure times establishes the relationship between gel moduli, $G'(t)$, and hydrogel autofluorescence, $B(t)$ (Figure 3c). Because $B(t)$ is linear with UV exposure time and $G'(t)$ follows first-order reaction kinetics, the relationship between $G'(t)$ and $B(t)$ is first-order as well and is given by

$$G'(B) = A\left[1 - e^{-\kappa(B-\delta)}\right] \quad (3)$$

The parameters for Figure 3c are as follows: A (Pa) is held to be the same from the fit in Figure 3a, κ represents how G' changes with brightness, and δ represents the brightness of a hydrogel exposed for delay time d, the time required for the onset of a measurable G'.

While the fit for $B(t)$ is accurate, it is not immediately clear why autofluorescent brightness would increase linearly with UV exposure time. Initially, it was expected that autofluorescence would also follow first-order reaction kinetics, similar to $G'(t)$. To explain this linear relationship, we further analyze the properties and structure of the hydrogel scaffold. Because hydrogel autofluorescence is caused by the restriction of motion of polymer chains as they are cross-linked into the gel network, we hypothesize that both hydrogel swelling and the amount of polymer included in the gel play a role in the resulting brightness.[39] Each of these components contributes directly to the volume fraction of polymer included in the gel structure. To begin to understand this correlation, we start by measuring the swelling ratio.

The swelling ratio is measured from gel images taken with the laser scanner, which are used to construct the calibration curve in Figures 3b,c. The area occupied by the gel in the image is determined by tracing the outer edges of the gel and counting the number of pixels included in the trace. This number is converted to an area using the pixel size, 25 × 25 μm. The swollen gel area ($A_{swollen}$) is used with the area of the unswollen gel ($A_{unswollen}$) to calculate a swelling ratio based on area, $Q_A = \frac{A_{swollen}}{A_{unswollen}}$. The area of a circle of diameter 6 mm is the area of an unswollen gel ($A_{unswollen}$) because the precursor

https://doi.org/10.1021/acs.macromol.2c00241
Macromolecules 2022, 55, 4469−4480

solution fills the PDMS ring in the sample chamber, which has a diameter of 6 mm. The volumetric swelling ratio, Q_V, is determined from Q_A by $Q_V = Q_A^{3/2}$ because swelling occurs isotropically as the hydrophilic PEG molecules attempt to maximize their contact with solvent. We assume isotropic swelling because the PDMS ring is removed, and the hydrogel is allowed to swell with no restriction in all directions. From the swelling ratio, we calculate the root-mean-squared end-to-end distance of the chains between neighboring cross-linking segments, $\langle r^2\rangle^{1/2}$. This measurement describes the amount of space available for polymers to move, which is an important component of aggregation-induced emission.[39,40,43]

$\langle r^2\rangle^{1/2}$ is calculated from the correlation length, ξ, and elongation ratio, α. ξ is the distance between neighboring polymer chains and α is related to the swollen gel polymer volume fraction. ξ is determined from the molecular weight between neighboring cross-links $\bar{M}_c$ using eqs 4 and 5

$$\frac{1}{\bar{M}_c} = \frac{\ln(1-\phi_s) + \phi_s + \chi\phi_s^2 - 2V_1\left[I^2 + \left(\frac{i\phi_s\rho_d}{2M_r}\right)^2\right]^{1/2} + 2V_1 I}{-1\left(1-\frac{2}{f}\right)(1-\gamma)V_1\rho_d\phi_r^{2/3}\phi_s^{1/3}} \tag{4}$$

$$\xi = \phi_s^{-1/3}\sqrt{\left(1-\frac{2}{f}\right)\bar{l}^2 C_\infty \frac{\lambda\bar{M}_c}{M_r}} \tag{5}$$

where ϕ_s is the volume fraction of polymer in the swollen state, χ is the polymer−solvent interaction parameter ($\chi = 0.426$ for PEG[57]), V_1 is the molar volume of water, I is the ionic strength of the solution, i is the degree of ionization of the polymer, ρ_d is the density of the polymer, M_r is molecular weight of the polymer repeat units, f is the polymer functionality ($f = 4$ for our backbone PEG molecule), γ is the frequency of chain defects, ϕ_r is the polymer volume fraction in the gel preswelling, C_∞ is the polymer characteristic ratio ($C_\infty = 6.8$ for PEG[58]), l is the length of an individual repeat unit ($\bar{l} = 0.35$ nm for PEG), and λ is the backbone bond factor ($\lambda = 3$ for PEG).[59−61] In our work, M_n is assumed to be 10 kDa, which accounts for two arms of the 4-arm 20 kDa PEG−norbornene molecule. We neglect terms in eq 4 that account for polymer charge and ionic strength, specifically $2V_1\left[I^2 + \left(\frac{i\phi_s\rho_d}{2M_r}\right)^2\right]^{1/2}$ and $2V_1 I$, because PEG is a neutral molecule and the ionic strength of our solution is low.

γ is estimated using Flory−Stockmayer theory.[30,62] The critical fraction of bonds that must form to initiate gelation, p_c, is

$$p_c = \frac{1}{\sqrt{(f_A-1)(f_B-1)/r}} \tag{6}$$

where r is the stoichiometric ratio between end-groups in the cross-linker and backbone molecules. For our scaffold, this is the ratio of thiol groups in the cross-linker to norbornene groups in the PEG backbone ($r = \frac{f_B n_B}{f_A n_A} = 0.65$). f_A is the functionality of the backbone molecule ($f_A = 4$), n_A are the moles of backbone, f_B is the functionality of the cross-linker ($f_B = 2$), and n_B are the moles of cross-linker. We use $\gamma = 1 - p_c$ to estimate the frequency of defects within the polymer gel. This method of determining γ likely overestimates the frequency of chain defects since it assumes that only the minimum number of cross-links are made to form the gel and that all other linkages form defects.

ϕ_s and ϕ_r are calculated using Q_V, and the concentration of polymer that is elastically contributing to the network, C_{poly}, is determined from the elastic moduli, G', by

$$G' = \left(1-\frac{2}{f}\right)C_{poly}RT \tag{7}$$

where f is the functionality of the polymer (for PEG−norbornene $f = 4$), R is the universal gas constant, and T is the absolute temperature.[63,64] Equation 7 only provides an estimate of the amount of elastically contributing polymer in the network and does not take into account the possibility of loop formation or other nonidealities that could be present in our network.[65,66] The formation of loops may contribute elastically to the measured G' to some extent and will restrict polymer motion in the partially reacted network, increasing autofluorescence. We are only using eq 7 to estimate separation distances between polymers in the gel from a measurement of elasticity. The elongation ratio α is related to ϕ_s by $\alpha = \phi_s^{-1/3}$, and $\langle r^2\rangle^{1/2}$ is calculated using[67]

$$\langle r^2\rangle^{1/2} = \frac{\xi}{\alpha} \tag{8}$$

Figure 4 shows the results of this calculation. In Figure 4, $\langle r^2\rangle^{1/2}$ decreases with increasing UV exposure time. This is

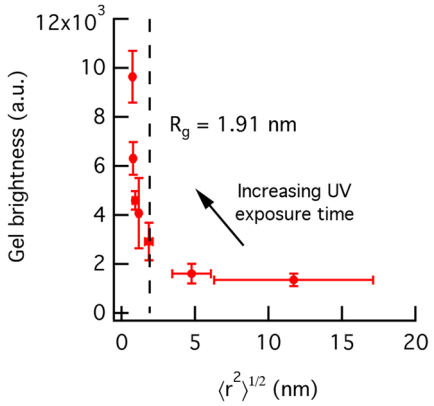

Figure 4. Gel autofluorescence, $B(t)$, as a function of the root-mean-squared end-to-end distance of the chains between neighboring cross-link segments, $\langle r^2\rangle^{1/2}$. Gels with large $\langle r^2\rangle^{1/2}$ have low autofluorescence while those with smaller $\langle r^2\rangle^{1/2}$ have higher autofluorescence. Brightness rapidly increases when $\langle r^2\rangle^{1/2}$ decreases below the radius of gyration, R_g, for a 4-arm star PEG, which is indicated by the vertical dashed line.

because gelation increases the cross-link density of the network, lowering the distance between neighboring cross-links. The increase in the cross-link density decreases the mobility of the polymer chains in the gel, increasing $B(t)$. The gel brightness increases as $\langle r^2\rangle^{1/2}$ is reduced and increases rapidly once $\langle r^2\rangle^{1/2}$ is reduced below the radius of gyration for our PEG molecule (R_g). R_g is the average space a polymer likely occupies when it is in a theta solvent and for our 4-arm PEG is equal to 1.91 nm.[30,62] When $\langle r^2\rangle^{1/2}$ is smaller than R_g, this increase in brightness occurs in samples that have similar

https://doi.org/10.1021/acs.macromol.2c00241
Macromolecules 2022, 55, 4469−4480

moduli. If $\langle r^2 \rangle^{1/2}$ were to be further reduced, possibly by increasing the amount of cross-linker in the reaction, we hypothesize that gel brightness would continue to increase. For this reason, the relationship between $\langle r^2 \rangle^{1/2}$ and gel brightness provides a possible explanation for brightness increasing linearly even after modulus has stopped changing during UV exposure.

Measuring Spatially Nonuniform Hydrogels. Using eq 3, we can now measure spatial variation in hydrogel elastic modulus. We begin by creating hydrogels with step changes in stiffness which are polymerized using the procedure outlined in the Interface Formation section. Three different interfaces are polymerized, and three gels are made per interface. Figure 5 shows the results of the calculated G' from autofluorescence measurements across a hydrogel with an interface between stiffnesses. The results in Figure 5 are measured by tracing the outer edges of the gel, which defines the perimeter, and analyzing the pixels inside the trace. From the trace, a rectangular sub-image is created which includes all of the points in the trace of the gel and some of its surroundings to form a rectangular image. This is done so that the image can be analyzed as a matrix. The highest and lowest values of x and y in the trace (i.e., the left- and rightmost points for x-coordinates and the top- and bottom-most points for y-coordinates) are used to define the bounds of the sub-image. The pixels inside the gel perimeter are converted from their brightness values to G' using the correlation in Figure 3c. This provides a matrix with entries of 0 Pa outside of the traced region and measurements of spatial variation in G' inside the traced gel region. The nonzero entries with the same x-value (corresponding to a single column in the matrix) are averaged to produce Figures 5a–c. Because we are averaging a roughly circular object, measurements near the left and right edges of the gel are less accurate because their averages include fewer pixels. For all interfaces made, the measurements of gel stiffness on each side of the interface agree between different gels made from different stock solutions. This demonstrates that the technique developed to create interfaces makes reproducible materials. Formal error propagation from the parameters in the model used to calculate G' is shown in the Supporting Information (Figure S6).

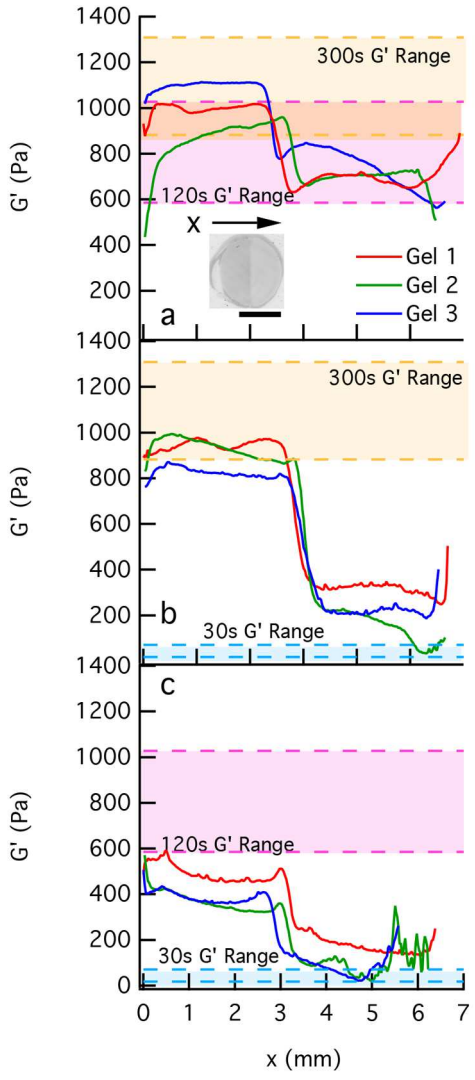

Figure 5. Moduli of gels that have a step change in stiffness or an interface. Exposure times for the gels are (a) 300 s/120 s, (b) 300 s/30 s, and (c) 120 s/30 s. The shaded regions represent the average ± one standard deviation for bulk rheological measurements of spatially uniform gels made at the same UV exposure time. An example of a 300 s/120 s gel image is provided as the inset of (a). Scale bar is 3 mm.

Figure 5a shows the results for the 300 s/120 s interface. Starting with the 300 s UV exposure side of the interface, we calculate G' values that agree between all gels, and these values fall within the range of values measured in uniform gels with bulk rheology. The same is true for the 120 s UV exposure side of the interface. Figures 5b,c have moduli measurements on either side of the interface that are consistent with one another. Some of these measurements are less consistent with bulk rheology measurements of uniform scaffolds at the same UV exposure time. In Figure 5b, the values of G' calculated for the 300 s UV exposure fall within or just below the values measured for uniform gels. G' values for the 30 s UV exposure side are higher than the values measured with bulk rheology. Additionally, in Figure 5c, the values for G' for the 120 s UV exposure time are below the expected range and values for G' on the 30 s UV exposure time are above the expected range. We hypothesize that the differences in measured G' on either half of the gel for both 300 s/30 s gels and the 120 s/30 s gels is due to radical diffusion under the photomask. As the reaction is occurring on the exposed side of the gel, radicals can diffuse into the unexposed region and start cross-linking before the side is exposed. This will result in a higher G' than expected, which agrees with the measurements in Figures 5b,c for the 30 s side. As radicals diffuse to the 30 s exposed side, fewer are available to react on the longer exposed side. This reduces the number of cross-links and the measured G' on the longer exposed side.

Diffusion of radicals to the unexposed side also provides an explanation for the difference between G' for the 30 s UV exposure halves of the 300 s/30 s gels and the 120 s/30 s gels. Because the UV exposure time difference between the two halves is greater for the 300 s/30 s gels, more time is available for radicals to diffuse to the unexposed side and increase its G'. This diffusion of radicals amounts to an increase of ∼150 Pa for the 300 s/30 s gels and ∼100 Pa for the 120 s/30 s gels. Additionally, 30 s is very close to the value of d when G' increases rapidly. This may also contribute to the discrepancies between G' across different gel sets, as small differences in radicals present can create large differences in G'. This

https://doi.org/10.1021/acs.macromol.2c00241
Macromolecules 2022, 55, 4469–4480

demonstrates a potential limitation of the technique for fabricating hydrogels with large G' differences. Another possible reason for the disagreement between these measured values is slight variations in the actual time the hydrogels are exposed. We believe this can contribute to the disagreement but may be a small factor because of the agreement between samples with the same interface.

To determine the thickness of the interface between the two different stiffnesses where G' is changing rapidly, we calculate the derivative dG'/dx where x is the distance along the gel perpendicular to the interface. The value of dG'/dx at point x_i where i refers to the x location within the gel is calculated using

$$\frac{dG'}{dx_i} = \frac{G'|_{x_i} - G'|_{x_{i-1}}}{\Delta x} \tag{9}$$

where Δx is the width of a pixel (25 μm) and $G'|_{x_i}$ and $G'|_{x_{i-1}}$ are the column-averaged G' values calculated from the scanning procedure described above. The results of this calculation for the three gels made with 300 s/120 s interfaces are shown in Figure 6. Results for 300 s/30 and 120 s/30 s interfaces are provided in Figure S5. The plot of dG'/dx is roughly zero on either side of the interface with the most significant variation occurring in a large negative spike near the center of the hydrogel. This spike represents the change in G' over the interface. Ideally, the change in G' would be instantaneous between the two halves of the gel. However, because of the experimental setup and polymerization technique, G' instead changes very rapidly over a small region of the hydrogel to form the interface. The "edges" of the interface, where G' stops changing rapidly, are defined as the first points immediately to the left and right of the sharp downward peak where $dG'/dx \geq 0$. Using the positions of these two points, we calculated the width of the interface. The widths of our interfaces are ~500 μm. We find that there are no statistically significant variations in the width of the interface when comparing gels made with each different set of UV exposure times. This indicates that our method consistently forms interfaces with similar thickness for the range of exposure time differences tested. The widths of these interfaces are larger than the typical cell size or length a cell can sense mechanical differences in the microenvironment but are similar to the width of interfaces found in the body such as mineralized cartilage in the patella.[68] In summary, consistent gels are made with interfaces in stiffness, and the measurement of G' using images of gel autofluorescence agrees well for gels with the same UV exposure times. While step changes in environmental stiffness will be encountered by cells as they migrate out of the scaffold and into the native tissue, many areas of the body have stiffness which changes gradually.[25] Similar gradients in our hydrogels can be made.

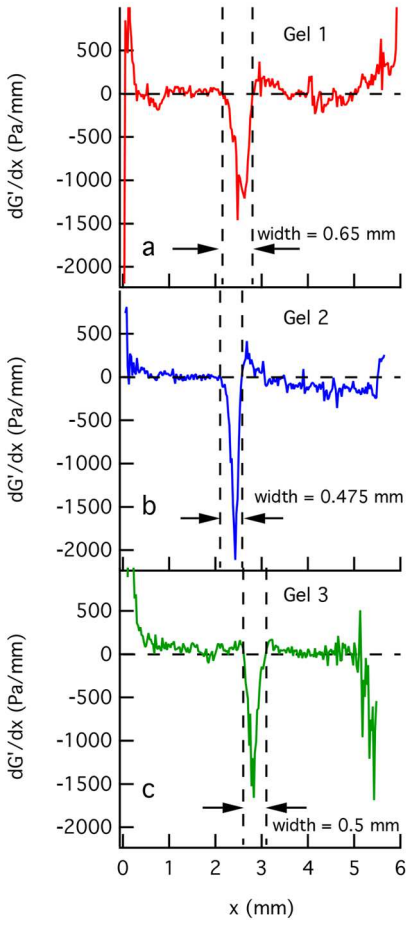

Figure 6. dG'/dx for (a–c) three 300 s/120 s gels. The large downward spike in the middle of the gel is the location of the interface.

UV exposure time can be varied in a continuous manner to form a smooth gradient in G'. To form a gradient in G', the UV exposure time is controlled by moving a photomask smoothly across the hydrogel precursor solution using a syringe pump. The photomask is attached directly to the syringe pump, and the pump rate is changed to move the photomask at different speeds. In this work we form three different gradients: (1) 180–30 s, (2) 120–30 s, and (3) 60–45 s. G' is calculated from a brightness measurement of the hydrogel using eq 3. This is the same way the stiffness of hydrogels with interfaces is calculated and is described in detail above. The results for how G' changes spatially in a gradient hydrogel are graphed in Figure 7.

Figure 7 shows the measurement of spatial variation of G' as a function of position across a hydrogel which is polymerized with a gradient in UV exposure time, resulting in a gradient in G'. Three gels (gels 1–3) are made from different stock solutions using identical experimental conditions, and their G' is calculated from the measured autofluorescence. The average value of G' from all three gels as a function of position is the yellow line, and the shaded region represents the standard deviation. Position x is the distance from the part of the hydrogel that is initially exposed to UV light. Finally, the theoretical G', which is the G' that would be measured if G' varied exactly as it does from the bulk rheology measurements (Figure 3a) and the gradient in UV exposure time is perfectly linear, is given for comparison. The formal error propagation from the parameters in the model used to calculate G' for gradient hydrogels is shown in the Supporting Information (Figure S7).

Figure 7a shows the calculated G' values across three hydrogels that are polymerized with a UV exposure gradient of 180–30 s. The average G' begins slightly below the theoretical value of G' for $x \lesssim 2.5$ mm but then agrees well with the theoretical curve for larger values of x. We hypothesize that the difference between the measured G' and theoretical value for small values of x is due to inaccuracies in the photomask

https://doi.org/10.1021/acs.macromol.2c00241
Macromolecules 2022, 55, 4469–4480

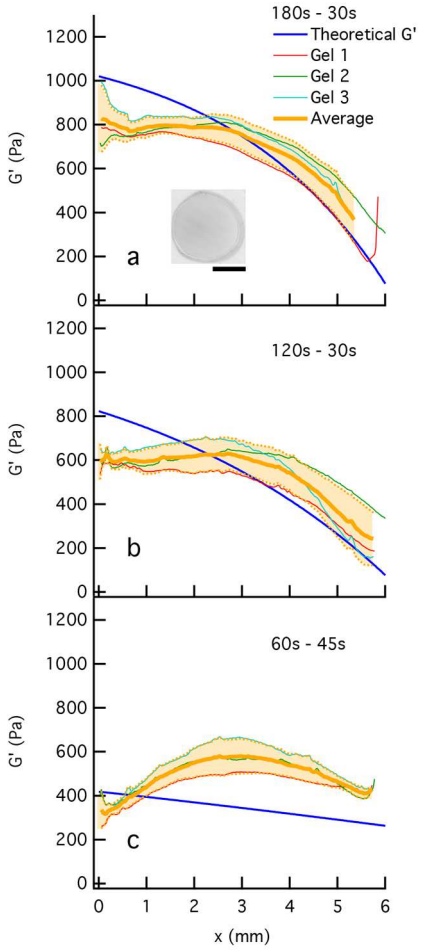

Figure 7. Calculation of G' from autofluorescence measurements of three sets of hydrogels with smooth gradients in UV light exposure time. Gradients are made by varying the maximum and minimum UV exposure time and are (a) 180−30 s, (b) 120−30 s, and (c) 60−45 s. The shaded region represents the average G' ± one standard deviation measured from the three hydrogels. An example of an image of a 180−30 s gel is provided as the inset of (a). Scale bar is 3 mm.

positioning during start-up. When the photomask is initially positioned, it is placed against a 3D-printed alignment attachment. Because the photomask is flexible, it could be flexed against the alignment attachment, allowing it to be pulled for a short time without actually moving enough to expose the precursor solution. Additionally, the syringe pump may not immediately move at the specified speed when it is started. These two issues when combined would result in a shorter UV exposure time and a lower G', which is measured for these hydrogels. After start-up, the measured G' values agree well with the theoretical G'. This demonstrates the importance of using a measurement to determine spatial variation in G' instead of just calculating the value of G' based on the experimental setup and ideal experimental conditions. A similar result is measured for 120−30 s gels in Figure 7b: a lower value of G' than the theoretical value is initially measured at start-up for $x \lesssim 2$ mm. This is likely due to flexing of the photomask and slower start-up speeds for the syringe pump. This is followed by good agreement between the measured G' and the theoretical G' for $x \gtrsim 2$ mm. For the 60−45 s hydrogels in Figure 7c we do not measure a gradient in G'. We hypothesize that this is due to the fact that the UV exposure time difference between each edge of the hydrogel is not very large and both the maximum and minimum UV exposure times are short. The resultant hydrogel has stiffness similar to one that is uniformly exposed at the average exposure time, ∼50 s. This shows a limitation in forming hydrogels with small gradients in G'. For steeper gradients, however, the results agree well with the theoretical values for G' after the initial start-up distance.

Limitations of the Technique. While this technique does quantify moduli accurately from images of autofluorescent brightness, it does have limitations and could be further developed to enable it to be used on a wider range of materials. A limitation of this technique is that it requires the samples to be transparent or near-transparent since it is an optical measurement. Autofluorescent brightness is likely affected by other variables such as sample thickness and type of solvent which were not investigated in this work. We suspect that thicker samples and higher viscosity solvents will result in more autofluorescent brightness. Thicker samples have more polymer which can contribute to the fluorescence, and higher viscosity solvents will restrict molecular motion more, increasing fluorescence. Additionally, the results presented here are specific to the selected hydrogel and laser scanner. A new calibration curve would have to be generated for each new material and for different laboratory equipment used to quantify brightness. It is likely, however, that the analysis can be made more general and apply to many different gels since the underlying physical phenomena that causes autofluorescence will be the same in each new system. This work provides a starting point for further development of the technique, including its validation with existing techniques such as atomic force microscopy and its use in characterizing new materials.

For this work, we have focused on characterizing G' using autofluorescence. Other rheological parameters such as the loss modulus, G'', and $\tan(\delta) = \frac{G''}{G'}$ are also quantifiable. We hypothesize that materials with higher G'' will have lower autofluorescence due to higher dissipation of stress and polymer mobility in the network. This would also result in an increase in $\tan(\delta)$ if G' is held constant. This is an opportunity for future work.

■ CONCLUSIONS

This work develops a new method for determining G' of a hydrogel from its autofluorescent brightness. G' and autofluorescence are measured for spatially uniform photopolymerizable hydrogels at varying UV exposure times. First, a relationship between G' and autofluorescence is developed. This relationship is related to the microstructure of the material, specifically, mobility of polymer chains in the gel network. As the extent of gelation increases, the amount of polymer cross-linked in the gel network increases and the swelling ratio decreases. This results in more restricted mobility of polymer chains, which leads to more autofluorescence by aggregation-induced emission. Using the relationship between G' and hydrogel autofluorescence, spatial variation in autofluorescence is measured, and the corresponding value of G' is calculated for nonuniform hydrogels. We polymerize hydrogels with both step changes and smooth gradients in G' and quantify the change in G' from images of gel autofluorescence. We show that hydrogels with consistent stiffness profiles can be made by controlling UV light exposure

https://doi.org/10.1021/acs.macromol.2c00241
Macromolecules 2022, 55, 4469−4480

spatially and that these complex materials can be effectively characterized using our relationship between G' and autofluorescence.

This technique provides a relatively simple method for characterizing nonuniform materials, which would otherwise be difficult or impossible to measure with existing techniques. This technique is based on relating a macroscale mechanical property, G', with the microscale structure and mobility of the polymer chains through measurements of autofluorescence. Hydrogel materials like those characterized in this work are especially relevant for tissue regeneration and wound healing applications. For effective cell delivery and to retain native cellular function, scaffolds used as implants should provide similar microenvironments to encapsulated cells as the native tissue. The technique described in this paper provides a method for fabricating and characterizing these spatially distinct materials that mimic complex environments in the body.

■ ASSOCIATED CONTENT

Supporting Information

The Supporting Information is available free of charge at https://pubs.acs.org/doi/10.1021/acs.macromol.2c00241.

Figure S1: frequency sweep data for all uniform hydrogels; Figure S2: representative images of uniform hydrogels; Figure S3: images of all interface hydrogels; Figure S4: images of all gradient hydrogels; Figure S5: dG'/dx for 300 s/30 and 120 s/30 s hydrogels; Figure S6: error propagation analysis for interface hydrogels; Figure S7: error propagation analysis for gradient hydrogels (PDF)

■ AUTHOR INFORMATION

Corresponding Author

Kelly M. Schultz − *Department of Chemical and Biomolecular Engineering, Lehigh University, Bethlehem, Pennsylvania 18015, United States;* orcid.org/0000-0001-9040-126X; Phone: +1 610 758 2012; Email: kes513@lehigh.edu

Author

John A. McGlynn − *Department of Chemical and Biomolecular Engineering, Lehigh University, Bethlehem, Pennsylvania 18015, United States*

Complete contact information is available at: https://pubs.acs.org/10.1021/acs.macromol.2c00241

Notes

The authors declare no competing financial interest.

■ ACKNOWLEDGMENTS

The authors thank Brian Slocum and the staff of The Wilbur Powerhouse for their assistance in creating the 3D prints used in this work. Funding for this work was provided by the National Science Foundation (NSF) under Grant CBET-1751057.

■ REFERENCES

(1) Loebel, C.; Mauck, R. L.; Burdick, J. A. Local nascent protein deposition and remodelling guide mesenchymal stromal cell mechanosensing and fate in three-dimensional hydrogels. *Nat. Mater.* **2019**, *18*, 883.

(2) Oliva, N.; Conde, J.; Wang, K.; Artzi, N. Designing hydrogels for on-demand therapy. *Acc. Chem. Res.* **2017**, *50*, 669−679.

(3) Hadden, W. J.; Young, J. L.; Holle, A. W.; McFetridge, M. L.; Kim, D. Y.; Wijesinghe, P.; Taylor-Weiner, H.; Wen, J. H.; Lee, A. R.; Bieback, K.; et al. Stem cell migration and mechanotransduction on linear stiffness gradient hydrogels. *Proc. Natl. Acad. Sci. U. S. A.* **2017**, *114*, 5647−5652.

(4) Chaudhuri, O.; Gu, L.; Klumpers, D.; Darnell, M.; Bencherif, S. A.; Weaver, J. C.; Huebsch, N.; Lee, H.-p.; Lippens, E.; Duda, G. N.; et al. Hydrogels with tunable stress relaxation regulate stem cell fate and activity. *Nat. Mater.* **2016**, *15*, 326.

(5) Boehnke, N.; Cam, C.; Bat, E.; Segura, T.; Maynard, H. D. Imine hydrogels with tunable degradability for tissue engineering. *Biomacromolecules* **2015**, *16*, 2101−2108.

(6) Purcell, B. P.; Lobb, D.; Charati, M. B.; Dorsey, S. M.; Wade, R. J.; Zellars, K. N.; Doviak, H.; Pettaway, S.; Logdon, C. B.; Shuman, J. A.; et al. Injectable and bioresponsive hydrogels for on-demand matrix metalloproteinase inhibition. *Nat. Mater.* **2014**, *13*, 653.

(7) Tokuda, E. Y.; Leight, J. L.; Anseth, K. S. Modulation of matrix elasticity with PEG hydrogels to study melanoma drug responsiveness. *Biomaterials* **2014**, *35*, 4310−4318.

(8) Anderson, S. B.; Lin, C.-C.; Kuntzler, D. V.; Anseth, K. S. The performance of human mesenchymal stem cells encapsulated in cell-degradable polymer-peptide hydrogels. *Biomaterials* **2011**, *32*, 3564−3574.

(9) Fairbanks, B. D.; Singh, S. P.; Bowman, C. N.; Anseth, K. S. Photodegradable, photoadaptable hydrogels via radical-mediated disulfide fragmentation reaction. *Macromolecules* **2011**, *44*, 2444−2450.

(10) Tan, H.; Chu, C. R.; Payne, K. A.; Marra, K. G. Injectable in situ forming biodegradable chitosan-hyaluronic acid based hydrogels for cartilage tissue engineering. *Biomaterials* **2009**, *30*, 2499−2506.

(11) Tibbitt, M. W.; Anseth, K. S. Hydrogels as extracellular matrix mimics for 3D cell culture. *Biotechnology and bioengineering* **2009**, *103*, 655−663.

(12) Ferreira, L. S.; Gerecht, S.; Fuller, J.; Shieh, H. F.; Vunjak-Novakovic, G.; Langer, R. Bioactive hydrogel scaffolds for controllable vascular differentiation of human embryonic stem cells Bioactive hydrogel scaffolds for controllable vascular differentiation of human embryonic stem cells. *Biomaterials* **2007**, *28*, 2706−2717.

(13) Burdick, J. A.; Anseth, K. S. Photoencapsulation of osteoblasts in injectable RGD-modified PEG hydrogels for bone tissue engineering. *Biomaterials* **2002**, *23*, 4315−4323.

(14) Raeber, G.; Lutolf, M.; Hubbell, J. Molecularly engineered PEG hydrogels: a novel model system for proteolytically mediated cell migration. *Biophys. J.* **2005**, *89*, 1374−1388.

(15) Lutolf, M.; Lauer-Fields, J.; Schmoekel, H.; Metters, A. T.; Weber, F.; Fields, G.; Hubbell, J. A. Synthetic matrix metalloproteinase-sensitive hydrogels for the conduction of tissue regeneration: engineering cell-invasion characteristics. *Proc. Natl. Acad. Sci. U. S. A.* **2003**, *100*, 5413−5418.

(16) Maxson, S.; Lopez, E. A.; Yoo, D.; Danilkovitch-Miagkova, A.; LeRoux, M. A. Concise review: role of mesenchymal stem cells in wound repair. *Stem cells translational medicine* **2012**, *1*, 142−149.

(17) Eggenhofer, E.; Luk, F.; Dahlke, M. H.; Hoogduijn, M. J. The life and fate of mesenchymal stem cells. *Front. Immunol.* **2014**, *5*, 148.

(18) Tse, J. R.; Engler, A. J. Stiffness gradients mimicking in vivo tissue variation regulate mesenchymal stem cell fate. *PloS one* **2011**, *6*, e15978.

(19) Engler, A. J.; Sen, S.; Sweeney, H. L.; Discher, D. E. Matrix elasticity directs stem cell lineage specification. *Cell* **2006**, *126*, 677−689.

(20) Han, L.; Grodzinsky, A. J.; Ortiz, C. Nanomechanics of the cartilage extracellular matrix. *Annu. Rev. Mater. Res.* **2011**, *41*, 133−168.

(21) Cox, T. R.; Erler, J. T. Remodeling and homeostasis of the extracellular matrix: implications for fibrotic diseases and cancer. *Disease models & mechanisms* **2011**, *4*, 165−178.

(22) Mikos, A. G.; Herring, S. W.; Ochareon, P.; Elisseeff, J.; Lu, H. H.; Kandel, R.; Schoen, F. J.; Toner, M.; Mooney, D.; Atala, A.; et al. Engineering complex tissues. *Tissue Eng.* **2006**, *12*, 3307−3339.
(23) Hoemann, C. D.; Lafantaisie-Favreau, C.-H.; Lascau-Coman, V.; Chen, G.; Guzmán-Morales, J. The cartilage-bone interface. *journal of knee surgery* **2012**, *25*, 085−098.
(24) Lynn, A. D.; Blakney, A. K.; Kyriakides, T. R.; Bryant, S. J. Temporal progression of the host response to implanted poly (ethylene glycol)-based hydrogels. *J. Biomed. Mater. Res., Part A* **2011**, *96*, 621−631.
(25) Seidi, A.; Ramalingam, M.; Elloumi-Hannachi, I.; Ostrovidov, S.; Khademhosseini, A. Gradient biomaterials for soft-to-hard interface tissue engineering. *Acta biomaterialia* **2011**, *7*, 1441−1451.
(26) Jackson, W. M.; Nesti, L. J.; Tuan, R. S. Concise review: clinical translation of wound healing therapies based on mesenchymal stem cells. *Stem cells translational medicine* **2012**, *1*, 44−50.
(27) Daviran, M.; Catalano, J.; Schultz, K. M. Determining how human mesenchymal stem cells change their degradation strategy in response to microenvironmental stiffness. *Biomacromolecules* **2020**, *21*, 3056−3068.
(28) Kyburz, K. A.; Anseth, K. S. Three-dimensional hMSC motility within peptide-functionalized PEG-based hydrogels of varying adhesivity and crosslinking density. *Acta biomaterialia* **2013**, *9*, 6381−6392.
(29) Leight, J. L.; Alge, D. L.; Maier, A. J.; Anseth, K. S. Direct measurement of matrix metalloproteinase activity in 3D cellular microenvironments using a fluorogenic peptide substrate. *Biomaterials* **2013**, *34*, 7344−7352.
(30) Larson, R. G. *The Structure and Rheology of Complex Fluids*, 1st ed.; Oxford University Press: 1998.
(31) Furst, E. M.; Squires, T. M. *Microrheology*; Oxford University Press: 2017.
(32) Schultz, K. M.; Furst, E. M. Microrheology of biomaterial hydrogelators. *Soft Matter* **2012**, *8*, 6198−6205.
(33) McGlynn, J. A.; Wu, N.; Schultz, K. M. Multiple particle tracking microrheological characterization: Fundamentals, emerging techniques and applications. *J. Appl. Phys.* **2020**, *127*, 201101.
(34) McConney, M. E.; Singamaneni, S.; Tsukruk, V. V. Probing soft matter with the atomic force microscopies: imaging and force spectroscopy. *Polym. Rev.* **2010**, *50*, 235−286.
(35) Costa, K.; Yin, F. Analysis of Indentation: Implications for Measuring Mechanical Properties With Atomic Force Microscopy. *J. Biomech Eng.* **1999**, *121*, 462.
(36) Allison, D. P.; Mortensen, N. P.; Sullivan, C. J.; Doktycz, M. J. Atomic force microscopy of biological samples. *Wiley Interdisciplinary Reviews: Nanomedicine and Nanobiotechnology* **2010**, *2*, 618−634.
(37) Wang, H.; Chu, P. K. *Characterization of Biomaterials*; Elsevier: 2013; pp 105−174.
(38) Monici, M. Cell and tissue autofluorescence research and diagnostic applications. *Biotechnology annual review* **2005**, *11*, 227−256.
(39) Xu, H.-X.; Tan, Y.; Wang, D.; Wang, X.-L.; An, W.-L.; Xu, P.-P.; Xu, S.; Wang, Y.-Z. Autofluorescence of hydrogels without a fluorophore. *Soft Matter* **2019**, *15*, 3588−3594.
(40) Mei, J.; Leung, N. L.; Kwok, R. T.; Lam, J. W.; Tang, B. Z. Aggregation-induced emission: together we shine, united we soar! *Chem. Rev.* **2015**, *115*, 11718−11940.
(41) Kwok, R. T.; Leung, C. W.; Lam, J. W.; Tang, B. Z. Biosensing by luminogens with aggregation-induced emission characteristics. *Chem. Soc. Rev.* **2015**, *44*, 4228−4238.
(42) Zhao, Q.; Sun, J. Z. Red and near infrared emission materials with AIE characteristics. *J. Mater. Chem. C* **2016**, *4*, 10588−10609.
(43) Luo, J.; Xie, Z.; Lam, J. W.; Cheng, L.; Chen, H.; Qiu, C.; Kwok, H. S.; Zhan, X.; Liu, Y.; Zhu, D.; et al. Aggregation-induced emission of 1-methyl-1, 2, 3, 4, 5-pentaphenylsilole. *Chem. Commun.* **2001**, 1740−1741.
(44) Daviran, M.; Longwill, S. M.; Casella, J. F.; Schultz, K. M. Rheological characterization of dynamic remodeling of the pericellular region by human mesenchymal stem cell-secreted enzymes in well-defined synthetic hydrogel scaffolds. *Soft Matter* **2018**, *14*, 3078−3089.
(45) Daviran, M.; Caram, H. S.; Schultz, K. M. Role of cell-mediated enzymatic degradation and cytoskeletal tension on dynamic changes in the rheology of the pericellular region prior to human mesenchymal stem cell motility. *ACS biomaterialsscience & engineering* **2018**, *4*, 468−472.
(46) Daviran, M.; Schultz, K. M. Characterizing the dynamic rheology in the pericellular region by human mesenchymal stem cell re-engineering in PEG-peptide hydrogel scaffolds. *Rheol. Acta* **2019**, *58*, 421.
(47) Mazzeo, M. S.; Chai, T.; Daviran, M.; Schultz, K. M. Characterization of the kinetics and mechanism of degradation of human mesenchymal stem cell-laden poly (ethylene glycol) hydrogels. *ACS Appl. Bio Mater.* **2019**, *2*, 81−92.
(48) McGlynn, J. A.; Druggan, K. J.; Croland, K. J.; Schultz, K. M. Human mesenchymal stem cell-engineered length scale dependent rheology of the pericellular region measured with bi-disperse multiple particle tracking microrheology. *Acta Biomaterialia* **2021**, *121*, 405−417.
(49) Schultz, K. M.; Kyburz, K. A.; Anseth, K. S. Measuring dynamic cell-material interactions and remodeling during 3D human mesenchymal stem cell migration in hydrogels. *Proc. Natl. Acad. Sci. U. S. A.* **2015**, *112*, E3757−E3764.
(50) Schultz, K. M.; Anseth, K. S. Monitoring degradation of matrix metalloproteinases-cleavable PEG hydrogels via multiple particle tracking microrheology. *Soft Matter* **2013**, *9*, 1570−1579.
(51) Fairbanks, B. D.; Schwartz, M. P.; Halevi, A. E.; Nuttelman, C. R.; Bowman, C. N.; Anseth, K. S. A versatile synthetic extracellular matrix mimic via thiol-norbornene photopolymerization. *Adv. Mater.* **2009**, *21*, 5005−5010.
(52) Fairbanks, B. D.; Schwartz, M. P.; Bowman, C. N.; Anseth, K. S. Photoinitiated polymerization of PEG-diacrylate with lithium phenyl-2, 4, 6-trimethylbenzoylphosphinate: polymerization rate and cytocompatibility. *Biomaterials* **2009**, *30*, 6702−6707.
(53) Hoyle, C. E.; Bowman, C. N. Thiol-ene click chemistry. *Angew. Chem., Int. Ed.* **2010**, *49*, 1540−1573.
(54) Aimetti, A. A.; Machen, A. J.; Anseth, K. S. Poly(ethylene glycol) hydrogels formed by thiol-ene photopolymerization for enzyme-responsive protein delivery. *Biomaterials* **2009**, *30*, 6048−6054.
(55) Lutolf, M. P.; Weber, F. E.; Schmoekel, H. G.; Schense, J. C.; Kohler, T.; Muller, R.; Hubbell, J. A. Repair of bone defects using synthetic mimetics of collagenous extracellular matrices. *Nat. Biotechnol.* **2003**, *21*, 513−518.
(56) Boggs, P. T.; Byrd, R. H.; Schnabel, R. B. A stable and efficient algorithm for nonlinear orthogonal distance regression. *SIAM Journalon Scientific and Statistical Computing* **1987**, *8*, 1052−1078.
(57) Merrill, E. W.; Dennison, K. A.; Sung, C. Partitioning and diffusion of solutes in hydrogels of poly (ethylene oxide). *Biomaterials* **1993**, *14*, 1117−1126.
(58) Young, R. J.; Lovell, P. A. *Introduction to Polymers*; CRC Press: 2011.
(59) Richbourg, N. R.; Peppas, N. A. The swollen polymer network hypothesis: Quantitative models of hydrogel swelling, stiffness, and solute transport. *Prog. Polym. Sci.* **2020**, *105*, 101243.
(60) Flory, P. J.; Rehner, J., Jr. Statistical mechanics of cross-linked polymer networks I. Rubberlike elasticity. *J. Chem. Phys.* **1943**, *11*, 512−520.
(61) Bray, J. C.; Merrill, E. W. Poly (vinyl alcohol) hydrogels. Formation by electron beam irradiation of aqueous solutions and subsequent crystallization. *J. Appl. Polym. Sci.* **1973**, *17*, 3779−3794.
(62) Rubinstein, M.; Colby, R. H.; et al. *Polymer Physics*; Oxford University Press: New York, 2003; Vol. *23*.
(63) Hoti, G.; Caldera, F.; Cecone, C.; Pedrazzo, A. R.; Anceschi, A.; Appleton, S. L.; Monfared, Y. K.; Trotta, F. Effect of the Cross-Linking Density on the Swelling and Rheological Behavior of Ester-Bridged β-Cyclodextrin Nanosponges. *Materials* **2021**, *14*, 478.

https://doi.org/10.1021/acs.macromol.2c00241
Macromolecules 2022, 55, 4469−4480

(64) Miller, D. R.; Macosko, C. W. A new derivation of postgel properties of network polymers. *Rubber chemistry and technology* **1976**, *49*, 1219−1231.
(65) Zhou, H.; Woo, J.; Cok, A. M.; Wang, M.; Olsen, B. D.; Johnson, J. A. Counting primary loops in polymer gels. *Proc. Natl. Acad. Sci. U. S. A.* **2012**, *109*, 19119−19124.
(66) Zhong, M.; Wang, R.; Kawamoto, K.; Olsen, B. D.; Johnson, J. A. Quantifying the impact of molecular defects on polymer network elasticity. *Science* **2016**, *353*, 1264−1268.
(67) Peppas, N.; Bures, P.; Leobandung, W.; Ichikawa, H. Hydrogels in pharmaceutical formulations. *Eur. J. Pharm. Biopharm.* **2000**, *50*, 27−46.
(68) Zizak, I.; Roschger, P.; Paris, O.; Misof, B.; Berzlanovich, A.; Bernstorff, S.; Amenitsch, H.; Klaushofer, K.; Fratzl, P. Characteristics of mineral particles in the human bone/cartilage interface. *J. Struct. Biol.* **2003**, *141*, 208−217.

https://doi.org/10.1021/acs.macromol.2c00241
Macromolecules 2022, 55, 4469−4480